IEEE Robotics and Automation Letters (RAL) paper presented at the
2020 IEEE International Conference on Robotics and Automation (ICRA)
31 May - 31 August, 2020. Paris, France

Characterizing Torso Stiffness in Female Adolescents with and without Scoliosis

Rosemarie C. Murray[1], Chawin Ophaswongse[1], Joon-Hyuk Park[2], and Sunil K. Agrawal[1],

Abstract— **Adolescent Idiopathic Scoliosis (AIS) is a spinal curvature that affects 3% of the population and disproportionately affects females. It is treated with bracing and many researchers are developing models of the torso to optimize the effectiveness of brace designs. Unfortunately, the data available to create these models is limited by the experimental methods employed. One method, in vitro spine cadaver stiffness measurements, is generally based on specimens from the elderly, which are not representative of the adolescent population. The other method, radiographic studies, can only provide a limited amount of information because of the radiation exposure that multiple images require. In this work, we present a Robotic Spine Exoskeleton (RoSE) tailored to the population in greatest need of AIS interventions–female adolescents. We use it to create a three-dimensional stiffness characterization of the torso in vivo for eight female adolescents with scoliosis and eight without this condition. The key findings include an interaction effect of DOF and torso segment on translational collinear stiffnesses, and an interaction effect of DOF and group on rotational collinear stiffnesses. We also found that the 3D coupling stiffness pattern is in line with that of the human spine, regardless of spinal deformity. Also, the magnitude of the torso stiffness for the tested population is less than that of the adult male population previously characterized. Our results provide quantitative data for torso stiffness and can be used to improve brace designs. Our methods could also be adapted as a way to customize subject-specific treatment methods, as there is a lot of variation among subjects.**

Prosthetics and Exoskeletons, Rehabilitation Robotics, Scoliosis, Medical Robots and Systems, Wearable Robots

I. Introduction

Adolescent Idiopathic Scoliosis (ALS) is a common spinal disorder that occurs in approximately 3% of the population [1]. It develops during adolescence, and while it can occur in both sexes, it disproportionately affects females, particularly in the more severe cases. It consists of an abnormal lateral curve as well as axial rotation of the spine, creating a three dimensional curvature. It is treated in two main ways; first, through bracing, and if that is not successful, through spinal fusion surgery. To resolve the three-dimensional nature of the curvature, both of these treatment techniques rely on an understanding of the three-dimensional stiffness of the spine within the torso structure.

Conservative treatment relies on prescribing rigid braces that hold the spine in the corrected position, and which can deter progression of the spinal curve when worn for 16+ hours/day until the adolescent reaches skeletal maturity. Unfortunately, if the conservative treatment fails to prevent curve progression beyond 50°, surgical intervention may be necessary to prevent further progression in adulthood [1]. While many studies have revealed the effectiveness of bracing, in general, it is still not clear how much force these braces apply to the body and how much force is required to change the position of the torso and spine [1]. Several studies have been done on the stiffness characterization of the spine in vitro, but little research has been done on the stiffness of the full torso-spine system in vivo. Too little force applied by the brace may not achieve the required position or force needed to curtail the curve progression. Too much force can cause discomfort, skin breakdown, and even deform the ribs [2]. Greater knowledge of the force-displacement characteristics of the torso-spine system may lead to better understanding of the nature of scoliosis and improved bracing and surgical techniques.

Some researchers have developed finite element models (FEM) or multi-body models (MBM) of the spine-torso system that promise to simulate the effects of bracing [3]. Techniques have been developed to personalize these models based on traction or lateral bending radiographs [4] or computed tomography [5]. FEM has been used in conjunction with CAD/CAM to create rigid TLSO's that provide greater in-brace correction with less surface covering and thinner material [6]. One problem with these models, however, is that they are based on either the material properties of the in vitro spine available in literature, or on radiographs under different loading conditions. The former may not match the characteristics of population in need of scoliosis treatment, since the specimens obtained were generally from elderly individuals and those undergoing scoliosis treatment are likely to be adolescents. The latter approach is limited in how much data can be provided because of the radiation risk, and might not be able to create a detailed characterisation.

Some work has been done on the creation of flexible bracing systems, which promise improved patient compliance resulting from improved comfort and quality of life over traditional rigid braces [7]–[10]. These devices aim to control the forces applied to the spine, rather than restricting its position. For this application, a detailed understanding of the stiffness characteristics of the torso is even more important, because the force on the torso must be calculated not just for one position, but for a localized area around the target position. Some evidence suggests that they may be effective for milder scoliotic curves, but less so with moderate to severe curvature [7]. Greater understanding of the stiffness characteristics of the torso may improve the design of these devices.

Prior work has evaluated the stiffness of the torso in rotation, but has failed to fully characterize the three-dimensional nature of the torso stiffness [11]. A full characterization of the coupling between forces and displacements is needed because scoliosis treatment involves precise repositioning of

the torso in multiple degrees-of-freedom at the same time. A moment applied about a particular axis may result not only in rotation about that axis, but also rotations about other axes and translation in three-dimensional space. To capture this complex relationship between force and displacement in the torso, one needs to calculate the 6×6 stiffness matrix of the torso. In addition, previous work has focused on the torso as a whole rather than separately articulating the lumbar and thoracic regions. However, with the development of the Robotic Spine Exoskeleton (RoSE), our group has previously presented a three dimensional stiffness of adult male torsos without spinal deformity, as well as a case study of an individual with kyphosis and an individual with scoliosis [12].

In this paper, we further explore the torso stiffness properties in individuals with scoliosis. Most cases of scoliosis develop during adolescence, and while there is strong evidence to support bracing treatment during adolescence, there is little compelling evidence that bracing in adults can improve curvature or prevent further progression [13]. Consequently, information about adolescent torso stiffness is more relevant to the current treatment that information about adults. In addition, scoliosis affects females more than males, and the ratio increases with the severity of the curve. Therefore, female adolescents are most at risk to develop curves that require surgical intervention. However, to the best of the authors' knowledge, the stiffness of the female adolescent spine or torso has not been characterized in vitro or in vivo. Here we characterize the three-dimensional stiffness of the torso in vivo in adolescent females with and without scoliosis. First, we will present the collinear stiffness values, then the three-dimensional stiffness matrices, followed by the correlation matrices. The collinear stiffness values allow us to broadly compare the effects of group, torso segment, and degree-of-freedom on the stiffness of the torso. The three-dimensional stiffness matrices provide data that can be used to convert between a set of displacements on the torso, and the set of forces required to achieve it. Finally the correlation matrices allow us to see how tightly coupled force and displacement are in each combination of degrees-of-freedom.

II. Methods

A. Robotic Spine Exoskeleton (RoSE)

The Robotic Spine Exoskeleton (RoSE) used for this experiment is a version of the design presented in [14], modified to fit adolescent females. As shown in Fig. 1, it consists of three rings around the torso connected in a double Stewart platform design. The rings are cut from an off-the-shelf thoracolumbar orthosis (Original Boston Brace, Boston Orthotics & Prosthetics, MA). The limbs are connected to the rings through attachments designed with CAD (Solidworks,MA) and 3D printed (Fortus 360mc, Stratasys, MN) in ABS. Each of the twelve limbs contains a linear actuator (L12-50-210-12-P, Actuonix, Canada). They have a 5 cm stroke length, a max speed of 6.2 mm/s, and a max force of 80 N. They are driven with TB6612FNG dual

Fig. 1. Robotic Spine Exoskeleton designed for adolescent females

Fig. 2. Upper Left: ring spacer; Lower Left: motor driver and multiplexer PCB; Right: motor housing.

motor driver (Toshiba, CA). The onboard potentiometers' signals are multiplexed and sent to the control board (myRio-1900, National Instruments, TX). The motors are placed in series with load cells (LCM200, Futek, CA). The signals from these load cells are amplified (CSG110, Futek, CA), and then multiplexed and delivered to the control board. The control board communicates wirelessly and provides a real-time control environment (Labview 2017, National Instruments, TX). Two custom-made printed circuit boards (Sunstone Circuits, OR), shown in Fig. 2, interface between the control board and the motors to drive the motors and multiplex potentiometer signals. The signals from the load cells are sent to a conditioning board (Mantracourt, ICA6H, UK) and then multiplexed with a custom circuit board. Another custom made circuit board regulates the voltage. Power to the control board is provided by a lithium polymer battery (7.4V, 2 Ah, Maxamps), and to the motors and other

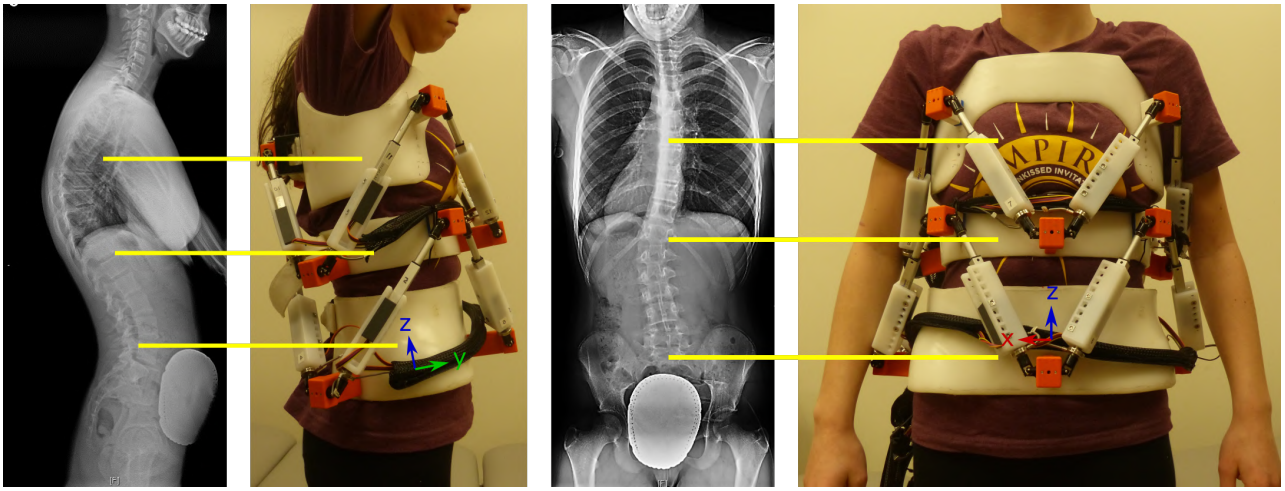

Fig. 3. Left to Right: Out of brace sagittal plane radiograph; side view of the subject in RoSE; out of brace coronal plane radiograph; front view of the subject in RoSE. The subject is 13 years old, with a 25° left lumbar curve and a 16° right thoracic curve.

electronics by a lithium polymer battery (18.5 V, 4 Ah, Maxamps).

The brace opens at the back and is fastened with a spacer from a set ranging in width from 2 to 12 cm, shown in in Fig. 2. In addition to ensuring the rigidity of each ring, the spacers allow us to adjust the perimeter of each ring by 10 cm to accommodate a wide variety of torso shapes and sizes. These adjustments also affect the locations of the limb attachment points. The relative position of the limb attachment points for each size of spacer was measured with motion capture (Vicon Motion Systems, UK) to ensure the inverse kinematics was correct for all settings. The change in limb attachment positions can also modify the available range of motion. To counteract this, the motors are housed in custom-milled UHMW housings (Proto Labs, MN) shown in Fig. 2. These housings allow the rest length of the limb to be adjusted by up to 4 cm in 1 cm increments. Given these adjustments, our device was able to fit subjects with a torso height (minimum distance from iliac crest to axilla) of 20 cm to 35 cm, and with torso perimeter measuring 69-81 cm at the iliac crest level, 66-79 cm at the xyphoid level, and 67-85 cm at the axilla level. The brace weighs 3.28 kg and is capable of at least 0.16 rad of rotation about each axis and 20 mm translation in each direction for each combination of ring sizes.

The control system is as described in [14]. Each level of the RoSE can be controlled independently. There are two methods of control - position and force. Both methods are structured in two levels: a high-level controller that sets the desired motor outputs based on the the desired position or wrench, implemented at 200 Hz, and a low level controller that sets the pulse width modulation for each motor based on the desired length or force calculated by the high-level controller, implemented at 500 Hz. The built-in potentiometers of the linear actuators and the load cells in each limb provide the feedback for closed-loop control in either mode. The joint position/force feedback is used to compute the real-time Cartesian position and forces on the brace levels. The controller's performance was validated on this hardware iteration using a motion capture camera system (Vicon Motion Systems, UK) and a six-axis force-torque sensor (Mini45, ATI Industrial Automation, NC).

B. Experiment Protocol

Sixteen female adolescent subjects were recruited, eight with scoliosis (age 13.0 ± 2.1 years, height 157 ± 6 cm, weight 45.3 ± 9.3 kg) and eight without scoliosis (age 17.3 ± 0.7 years, height 162 ± 5 cm, weight 52.3 ± 4.9 kg). Informed consent was obtained from all subjects, and the study was approved by the Columbia Institutional Review Board. None of the subjects had a history of spine injuries, cardiopulmonary conditions, neurological or physical impairments, or other orthopedic impairments that might affect the spine and torso. The control group also did not have a history of back pain or spinal deformity. The subjects wore the brace while seated, and it applied small displacements to the torso, and measured the resulting force. The data collection protocol was similar to that described in [12], summarized and with differences noted here.

Subjects were measured and the brace was adjusted to their height and width. Any gaps between the body and the brace were filled with closed cell foam up to 3/8 inch thick. Subjects were comfortably seated on a stool throughout the data collection, and were instructed to relax and neither exaggerate nor resist the motion of the brace. A representative subject with scoliosis is shown in Fig. 3. Her out-of-brace radiographs are juxtaposed with images of her wearing the RoSE to illustrate the alignment of the device with the body.

Displacements were applied in two conditions: first, with the middle and top ring fixed relative to each other and moving together relative to the bottom ring; and second, with the bottom and middle ring fixed relative to each other and the top ring moving independently. For each

condition, six displacements were applied in each degree-of-freedom. Displacement increments were determined by the subject's comfortable range of motion. Ideally, subjects received displacements of -15, -10, -5, 5, 10 and 15 mm in translation, and -0.15, -0.10, -0.05, 0.05, -0.10, and -0.15 radians in rotation. However, if the subject expressed discomfort at the extremes of this range, the displacements were reduced to -12, -8, -4, 4, 8, and 12 mm in translation, or -0.12, -0.08, -0.04, 0.04, 0.08, and 0.12 radians in rotation. The actual position was recorded simultaneously with the force and moment data and used for analysis. Three cycles of displacement were performed at each of the displacement positions, and the mean of the measured force and displacement was used for the analysis. A displacement cycle consisted of 1 second of translation to the new position, 2 seconds of maintaining the position and recording the resultant forces and moments, 1 second of data collection, 1 second of returning to the neutral position, and finally a 1 second pause before beginning the next cycle. During the one second data collection, both position and forces/moments were recorded at 100 Hz. During the pause in the neutral position, the load cells were tared so that residual forces and moments would be accounted for. The data collection is shown in the accompanying supplementary video.

C. Data Analysis

To see whether our control and scoliosis groups differed in any significant way other than spinal condition, we used a 2 sample t-test to determine whether the groups were significantly different in terms of age, height, or weight. The data was then analyzed to determine whether the force was linearly related to the displacement. To do this, we calculated the adjusted coefficent of determination (adjusted r-squared value) for the collinear force-displacement plot for each subject.

After confirming that the assumption of linear stiffness held for this group, we computed the collinear stiffness values in each dimension for both groups. The distribution of collinear stiffness values was tested for normality using the Shapiro-Wilk tests. A three way mixed model Analysis of Variance (ANOVA) with two between factors (group: control and scoliosis; thorax level: upper and lower) and one within factor (degree-of-freedom: x, y, and z) was applied. This model was applied separately to translational and rotational degrees-of-freedom. Leven's and Mauchly tests were used to explore variance and Sphericity of data. Greenhouse-Geisser correction was used in case sphericity assumption was violated. The significance level was set at an alpha rate of 0.05. Posthoc testing was analyzed only if the ANOVA model was significant (omnibus test). Bonferroni's inequality procedure was applied to adjust p-values and control the familywise error rate. Additionally, the statistical power of the ANOVA models are addressed in case of statistical significance.

We then constructed the three-dimensional stiffness matrix for each subject, non-dimensionalized and normalized it, and then found the mean and standard deviation across the group.

TABLE I

ADJUSTED COEFFICIENT OF DETERMINATION FOR COLLINEAR STIFFNESSES

	Control		Scoliosis	
	Lumbar	Thoracic	Lumbar	Thoracic
k_x	0.97 ± 0.05	0.98 ± 0.03	0.97 ± 0.04	0.94 ± 0.07
k_y	0.99 ± 0.01	0.99 ± 0.01	0.99 ± 0.01	0.99 ± 0.01
k_z	0.97 ± 0.02	0.97 ± 0.01	0.97 ± 0.01	0.94 ± 0.06
k_ϕ	0.87 ± 0.22	0.89 ± 0.11	0.95 ± 0.07	0.91 ± 0.13
k_θ	0.93 ± 0.08	0.94 ± 0.11	0.94 ± 0.04	0.96 ± 0.03
k_ψ	0.91 ± 0.07	0.94 ± 0.05	0.94 ± 0.04	0.97 ± 0.02

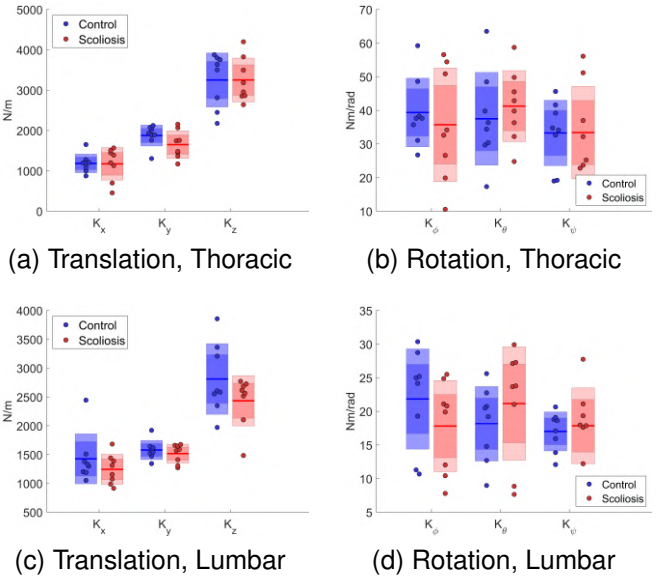

Fig. 4. Magnitudes of collinear stiffnesses. Data from the control group is shown in blue, and data from the scoliosis group is shown in red. Plots (a) and (c) show translational stiffnesses, while (b) and (d) show rotational stiffnesses. Plots (a) and (b) are from the thoracic level, while plots (c) and (d) are from the lumbar level. Stiffness values of individuals are represented by points, while the group mean is shown as the center line. The lightly shaded box represents the one standard deviation of the mean, and the heavily shaded inner box represents 95% confidence interval of the mean.

Next, we re-normalized and re-dimensionalized the group stiffness matrix to retrieve its real-world significance. This process is detailed in [12] and summarized in the appendix. Each term in the normalized stiffness matrix was tested for normality using the Shapiro-Wilkes test. Each term was then tested for significant difference from zero using either a one-sample t-test or Wilcoxon signed rank test depending on whether the distribution was normal.

III. RESULTS

A. Collinear Stiffnesses

For both groups at both levels of the trunk, there existed a strong linear relationship between force and displacement. The linear model was a good fit, with an adjusted coefficient of determination of at least 0.87 for every direction in each group and level. Average adjusted coefficient of determinations are reported for each DOF in Table I. The two groups had significantly different mean ages (2 sample t-test with unequal variance, p = 0.006). The groups did not have significantly different heights or weights. We then

TABLE II

GROUP COLLINEAR STIFFNESSES

	Control		Scoliosis	
	Lumbar	Thoracic	Lumbar	Thoracic
k_x [N/m]	1416 ± 74	1217 ± 79	1205 ± 86	1199 ± 128
k_y [N/m]	1600 ±89	1542 ±89	1885 ±59	1669 ±67
k_z [N/m]	2812 ±65	2378 ±51	3286 ±198	3270 ±128
k_ϕ [Nm/rad]	21 ±2	17 ±2	38 ±1	32 ±4
k_θ [Nm/rad]	18 ±1	21 ±2	38 ±3	43 ±2
k_ψ [Nm/rad]	17 ±1	17 ±1	33 ±2	32 ±2

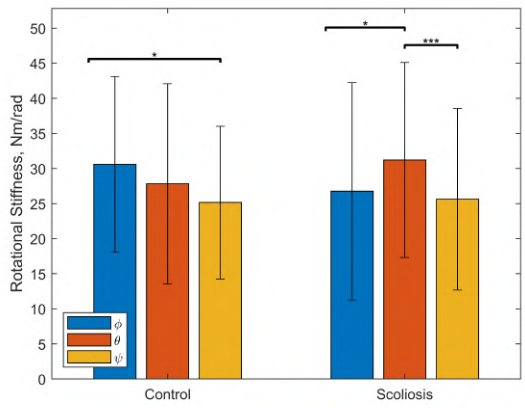

Fig. 5. Rotational stiffness for combined thoracic and lumbar levels in control and scoliosis groups. Bars show significant differences between groups (* represents $p < 0.05$, ** represents $p < 0.01$, and *** represents $p < 0.001$)

tested whether age correlated with collinear stiffness in any degree-of-freedom at either segment of the torso. We found that the age was only significantly correlated with collinear stiffness in the y-direction at the thoracic segment (p=0.013), and increased on average 78 N/m per year. However, due to the fact that only one outcome out of twelve was correlated with age, we did not analyze its effects further.

The mean collinear stiffness values are given in Table II, and their spread is shown in Fig. 4. The Shapiro-Wilk test for normality indicated that distribution was normal for all groups and directions, except the control group in the x-direction of the lumbar region and the y-direction of the thoracic region, and for the scoliosis group in the z-direction of the lumbar region. During translations, the statistical analysis showed an interaction effect between DOF and torso segment on stiffness ($F(1.6, 44.98) = 11.77$, $p = 0.000$, power = 0.72). Significant differences in stiffness between lumbar and thoracic regions were observed within y-translation (Thoracic = 1764 (SD:316), Lumbar = 1548 (SD:162), $p = 0.02$) and within z-translation (Thoracic = 3253 (SD:589), Lumbar = 2623 (SD:550), $p = 0.02$). This differs from observations on the stiffness in adult males, in which the lumbar region had greater stiffness for all degrees-of-freedom. Within either lumbar or thoracic segments, all DOFs were different with respect to each other. The relative magnitudes of the translational stiffnesses, $k_x < k_y < k_z$, were generally in line with prior research on the human spine segments [15]–[18], but differed somewhat from the relative torso stiffnesses of adult males [12], which was $k_y < k_x < k_z$.

During rotations, an interaction effect between DOF and group for stiffness was found ($F(2, 56) = 3.70$, $p = 0.031$, power = 0.66). No differences in stiffness were found between control and scoliosis groups (ϕ rotation, $p = 0.334$; θ rotation, $p = 0.348$, and ψ rotation, $p = 0.882$). However, the DOFs were significantly different within groups, as shown in Fig. 5, in differing patterns between the scoliosis and control groups.

Overall, the stiffness of the torso was about two orders of magnitude smaller than the spine itself in translational degrees-of-freedom, but about one order of magnitude less stiff in the rotational degrees-of-freedom [15]–[18]. It is also somewhat lower than the torso stiffness of adult males measured in [12]. This difference is consistent with findings that adult male spinal disks have greater compressive stiffness than adult female spinal disks in vitro [19]. Males would be expected to have more well developed musculature than females, which would be expected to increase stiffness as well. Age may also play a role, as changes to the skeleton and muscles during maturation could affect the torso stiffness.

B. Stiffness Matrices

The three-dimensional stiffness characterization for each group at each level is presented in Fig. 6. The 6×6 stiffness matrices contains the collinear stiffness terms along the diagonal and the coupling stiffness between different degrees-of-freedom in the off-diagonal terms. As expected, the group average stiffness matrices were not symmetric. This is in agreement with properties observed in human spine segments [20], as well as in adult male torsos [12], and is supported by the fact that spine, ligaments, muscles, and other soft tissues have some viscous properties, in addition to potential nonconservative contributions to the force provided by contact forces in the facet and costovertebral joints, and activation forces from the muscles and ligaments in the torso.

C. Correlation Matrices

Kendall's rank correlation coefficient was calculated to assess the correlation between forces and displacements in all directions, shown in Fig. 7. Kendall's was preferred to Pearson's rank correlation coefficient because the distribution of displacements did not follow a normal distribution for all degrees-of-freedom. Correlations that are statistically different from zero are marked with asterisks (* $p < 0.05$, ** $p < 0.01$). The diagonal terms of each matrix are the collinear force-displacement relationships, and are strongly correlated for both groups at both levels, as expected. Many of the off-diagonal terms are also strongly correlated, particularly terms k_{51}, k_{42}, k_{24}, and k_{15}. This set of terms is referred to as the primary coupling, and would be expected due to the pelvis being fixed. For example, in k_{51}, translating the torso in the x-direction relative to the pelvis would be expected to create a lateral bending moment. This set of couplings is strong ($\tau > 0.5$) for both groups and both levels, and can also be found in the stiffness matrix of the spine itself [18].

	Tx	Ty	Tz	Rx	Ry	Rz
Fx	1205 ±86	-25 ±51	-90 ±70	-28 ±14	-194 ±16	-25 ±11
Fy	74 ±48	1885 ±59	105 ±193	181 ±26	-14 ±10	-45 ±17
Fz	51 ±54	-31 ±120	3286 ±198	63 ±17	7 ±12	15 ±8
Mx	-2 ±6	208 ±14	86 ±12	38 ±1	3 ±2	-1 ±2
My	-97 ±5	-9 ±5	15 ±17	3 ±2	38 ±3	5 ±2
Mz	-25 ±12	-31 ±10	36 ±12	-2 ±2	2 ±3	33 ±2

(a) Control Group, Thoracic

	Tx	Ty	Tz	Rx	Ry	Rz
Fx	1199 ±128	-141 ±57	8 ±66	-40 ±8	-139 ±10	-8 ±18
Fy	17 ±48	1669 ±67	242 ±73	140 ±14	5 ±9	-59 ±13
Fz	72 ±38	60 ±44	3270 ±128	51 ±16	26 ±17	26 ±9
Mx	-20 ±6	172 ±8	23 ±21	32 ±4	4 ±1	-6 ±1
My	-77 ±4	19 ±7	23 ±9	2 ±1	43 ±2	4 ±2
Mz	-28 ±8	-43 ±11	29 ±19	-3 ±2	-0 ±2	32 ±2

(b) Scoliosis Group, Thoracic

	Tx	Ty	Tz	Rx	Ry	Rz
Fx	1416 ±74	78 ±38	139 ±62	-6 ±6	-56 ±10	-6 ±7
Fy	11 ±35	1600 ±89	57 ±98	92 ±10	14 ±5	-8 ±7
Fz	202 ±40	8 ±70	2812 ±65	34 ±21	-2 ±5	5 ±7
Mx	-7 ±5	82 ±8	30 ±20	21 ±2	-1 ±1	-2 ±1
My	-50 ±8	9 ±3	-23 ±3	0 ±1	18 ±1	4 ±1
Mz	-21 ±8	-11 ±3	-8 ±7	0 ±1	2 ±1	17 ±1

(c) Control Group, Lumbar

	Tx	Ty	Tz	Rx	Ry	Rz
Fx	1217 ±79	8 ±49	-129 ±80	-9 ±8	-36 ±18	-2 ±7
Fy	21 ±46	1542 ±89	-13 ±45	75 ±6	9 ±5	-9 ±5
Fz	26 ±56	-75 ±49	2378 ±51	20 ±16	4 ±7	13 ±7
Mx	-6 ±5	73 ±5	21 ±14	17 ±2	-1 ±1	-1 ±1
My	-33 ±4	6 ±5	-26 ±9	-0 ±0	21 ±2	3 ±1
Mz	-23 ±5	-6 ±4	-5 ±12	-0 ±1	2 ±1	17 ±1

(d) Scoliosis Group, Lumbar

Fig. 6. Mean $\pm$ the standard deviation of the rescaled stiffness matrices by group and torso segment. Stiffness matrices for the thoracic level are shown in (a) and (b), while the lumbar level is shown in (c) and (d). The average stiffness matrices for the control group are shown in (a) and (c), while (b) and (d) show the averages for the scoliosis group. The units for the upper left quadrant of each matrix is [N/m], the upper right and the lower left quadrants is [N], and the bottom right quadrant is [Nm/rad].

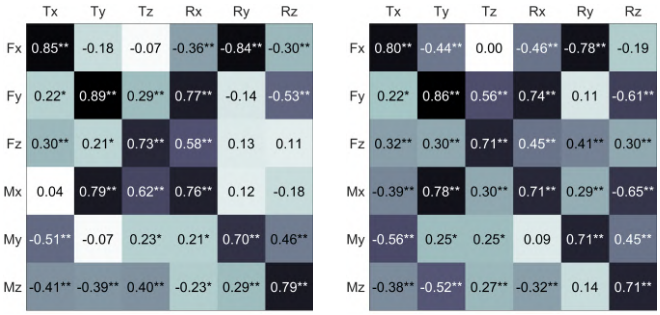

(a) Control Group, Thoracic

(b) Scoliosis Group, Thoracic

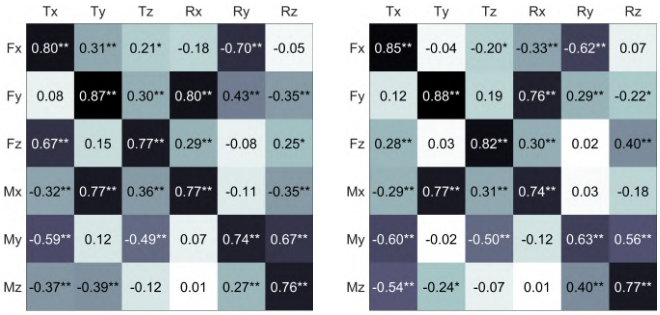

(c) Control Group, Lumbar

(d) Scoliosis Group, Lumbar

Fig. 7. Correlation matrices by group and torso segment. The correlation matrices for the thoracic level are shown in (a) and (b), while the lumbar level is shown in (c) and (d). The correlation matrices for the control group are shown in (a) and (c), while (b) and (d) are for the scoliosis group. Asterisks mark correlations that are significantly different from zero ($*p < 0.05$, $**p < 0.01$). Cell shading is on a gradient from weakest correlation (white) to strongest correlation (black).

Some additional off-diagonal terms show strong correlations in one or more of the groups and levels. For the control group, this is k_{26}, k_{34}, and k_{43} at the thoracic level and k_{31} and k_{56} at the lumbar level. For the scoliosis group, this is k_{23}, k_{26}, k_{46} and k_{62} at the thoracic level and k_{53} and k_{56} at the lumbar region. Some of these couplings, for example, $k_{23}, k_{34}, k_{43}, k_{56}$ and k_{61}, may be due to the posterior displacement of the spine, which is the stiffest element in the torso. For example, a displacement applied in the x-direction may displace the ribs and center of the torso more easily than the spine at the back of the torso, and thereby create a moment about the z-axis (k_{61}). Finally there may be some additional strong correlations that relate to the curves in the spine itself. In the thoracic region, both groups have a strong correlation at k_{26}. In the lumbar region, the correlation in k_{53} could be related to the natural lordosis of the lumbar spine flattening out during extension. In the scoliosis group, the terms k_{46} in the thoracic region is an out of plane coupling that may be due to the scoliotic curve.

IV. Discussion

A. Clinical Implications

We found that collinear stiffnesses of the female adolescent torso to be similar to the human spine in terms of relative magnitude, although lower in magnitude overall. In addition, the collinear stiffness were not significantly different between the two groups, although there was an interaction effect between group and DOF in the rotational stiffness. This indicates that it may be relatively more difficult for someone with scoliosis to bend laterally than to bend in flexion/extension, as compared to someone without scoliosis. We found that the three dimensional coupling stiffness characteristics of the torso are comparable to those of the human spine, irrespective of AIS. While it might be assumed that this type of spinal deformity would create significant changes in the population in terms of the collinear stiffnesses or the coupling stiffness characteristics, AIS is highly individualized. Individual differences may be more salient than generalized comparison between the AIS population as a whole and the typically developing population.

The findings also suggest that the torso stiffness of female adolescents is different in magnitude from that of adult males. The differences between this population and those previously studied underscore the importance of using data gathered from this group in order to design interventions intended for them. Overestimating the torso stiffness could result in brace designs that apply too much force and create discomfort or injury.

B. Applications

This data provides a benchmark which could be used for validating FEM models of the torso. In particular, it provides a helpful frame of reference for working with adolescent patients, who are not well represented in prior work on the spine in vitro or the torso in vivo, and who may have different material properties of the torso than adults. In addition, these results can inform the design of scoliosis braces. The stiffness matrix allows one to calculate the effects of forces and moments applied in multiple directions on rotation and displacement of the torso, and vice versa. This can allow rigid orthoses manufacturers to better understand the amount of force applied to the torso by a given orthosis design. For the manufacturers of flexible orthoses, the stiffness matrix data can help them better estimate the amount of tension needed in straps to ensure that sufficient correction is achieved, as well as improve the placement of the straps. Finally, the device and methodology presented provide a strategy for quickly and easily obtaining detailed data on the stiffness characteristics of an individual without subjecting them to radiation, which could be incorporated into the design of individualized scoliosis braces in the future.

C. Limitations and Future Work

The results of this study shed light on the stiffness of the torso in female adolescents and the forces/moments required to create specific displacements. However, to truly understand how forces applied to the torso affect the displacement of the spine, it is necessary to image the spine itself during these procedures. Such technology is available in the form of EOS imaging systems, which use low-dose dual-plane x-rays to reproduce the 3D position of the spine with a fraction of the radiation of a traditional chest x-ray. In addition, the study was restricted to quasi-static analysis of the torso stiffness. However, the dynamic properties of the torso may also be of interest, because the soft tissues of the torso do not behave in a purely elastic way.

In this study, there was a difference in the mean age of the two groups. However, within each group, there was no significant correlation between age and collinear torso stiffness terms at the upper or lower level of the torso, which allowed us to neglect age in our analysis. Adolescence is a period of rapid change, and it may be possible that there is an effect of age that we were unable to detect. Further, we did not have a way to measure skeletal maturity, a factor correlated with age but which has a strong influence on the likelihood of progression in scoliosis, and which would be expected to affect spinal stiffness. It may be informative to run a longitudinal study to see how individual's torso properties change over time in this population, and to correlate that with a metric of skeletal maturity, such as the Risser sign.

Another limitation on the present study is that the relationship between torso stiffness and muscle activation is not well understood. We were unable to capture this aspect through surface electromyography because of the limited area on which electrodes could be placed while the device was worn. This area is further reduced during bending, and the procedure entailed bending in every direction, so there were no locations suitable to place electrodes on the user during the experiment. To provide consistency in this experiment, subjects were instructed to relax as much as possible. However, if possible, it may be useful to measure how the muscles activate in response to forces applied to the torso, and how that affects the measured stiffness.

Despite the limitations present, the stiffness characterization can enable us to use the RoSE to study physical therapy interventions in posture rehabilitation. For example, we can design paradigms that allow us to apply a corrective force in some degrees-of-freedom, and anticipate the effects of that force on posture change both in the desired degree-of-freedom and other directions as a result of stiffness coupling. We could modulate these forces as subjects move through a variety of postures in order to encourage them to recognize a range of desirable postures rather than one static pose. Alternatively, we could apply forces opposite to the direction of desired direction of displacement, in order to train the subject to resist and strengthen their muscles.

V. Conclusion

In this paper, we present a variation of the Robotic Spine Exoskeleton tailored to female adolescents: a population underrepresented in literature on the spine/torso despite being the most affected by AIS. We use the RoSE to characterize the stiffness of the torso in eight female adolescents with scoliosis, and eight without. The key findings include the collinear stiffnesses, which had an interaction effect between torso segment and degree-of-freedom in translation and between group and degree-of-freedom in rotation; and the three dimensional coupling stiffness characteristics of the torso, which are comparable to those of human spine, irrespective of spinal deformity. This data can be used to validate FEM models of the torso and inform the design of scoliosis braces.

VI. Acknowledgements

We thank Rebekah Wallach, DPT; Prachi Bakarania, DPT; and Aruna Chavali for their help with subject recruitment.

Appendix I
Stiffness Matrix Calculation

First, the stiffness matrix, K, was calculated for each subject at each level, by solving the equation $\mathbf{F} = \mathbf{K}\Delta\mathbf{X}$, where $\Delta\mathbf{X}$ is the displacement vector applied to the subject ($\Delta\mathbf{X} = [\Delta x, \Delta y, \Delta z, \Delta\phi, \Delta\theta, \Delta\psi]^T$) and $\mathbf{F}$ is the vector of forces and moments measured in response ($\mathbf{F} = F_x, F_y, F_z, M_x, M_y, M_z]^T$).

$$\begin{bmatrix} F_x^{(1)} & \dots & F_x^{(n)} \\ \vdots & \ddots & \dots \\ M_z^{(1)} & \dots & M_z^{(n)} \end{bmatrix} = \begin{bmatrix} k_{11} & \dots & k_{16} \\ \vdots & \ddots & \dots \\ k_{61} & \dots & k_{66} \end{bmatrix} \times \begin{bmatrix} \Delta x^{(1)} & \dots & \Delta x^{(n)} \\ \vdots & \ddots & \dots \\ \Delta\psi^{(1)} & \dots & \Delta\psi^{(n)} \end{bmatrix} \quad (1)$$

where the superscript (i) denotes the i^{th} force-displacement measurement. The system of equations was solved simultaneously using *linsolve* (MATLAB, MathWorks). The subject's stiffness matrix was then transformed to a dimensionally uniform matrix, and then normalized, before being averaged element-wise over the group.

The dimensions of the stiffness matrix are N/m in the top left quadrant, Nm in the bottom right quadrant, and N in the remaining regions. In order to normalize the matrix, the terms must first be dimension matched. To do this, the force and position vectors ($\mathbf{F}$ and $\mathbf{X}$) are converted to dimensionally uniform vectors ($\tilde{\mathbf{F}}$ and $\tilde{\mathbf{X}}$) by pre-multiplying the conversion matrices ($\mathbf{D_F}$ and $\mathbf{D_X}$):

$$\begin{aligned} \tilde{\mathbf{F}} &= \mathbf{D_F}\mathbf{F} \\ \tilde{\mathbf{X}} &= \mathbf{D_X}\mathbf{X} \end{aligned} \quad \text{where} \quad \begin{aligned} \mathbf{D_F} &= \text{diag}(1,1,1,L^{-1},L^{-1},L^{-1}) \\ \mathbf{D_X} &= \text{diag}(1,1,1,L,L,L) \end{aligned} \tag{2}$$

where the characteristic length, L, is the maximum radius of the pelvic ring from its geometric center to the limb attachment points ($0.14m$). Substituting these dimensionally uniform matrices into the equation $\mathbf{F} = \mathbf{K}\Delta\mathbf{X}$, we get $\mathbf{F} = \mathbf{D_F}\mathbf{K}\mathbf{D_X^{-1}}\Delta\tilde{\mathbf{X}}$, and can then obtain the dimensionally uniform matrix, $\tilde{\mathbf{K}}$:

$$\tilde{\mathbf{K}} = \mathbf{D_F}\mathbf{K}\mathbf{D_X^{-1}} \tag{3}$$

Each dimensionally uniform stiffness matrix was then normalized to its Frobenius norm, $||\tilde{\mathbf{K}}||_F$, which represents the overall magnitude of the matrix; in other words, the aggregate stiffness. The resulting normalized stiffness matrix, $\hat{\mathbf{K}}$, is as follows:

$$\left|\left|\tilde{\mathbf{K}}\right|\right|_F = \sqrt{tr(\tilde{\mathbf{K}}^{\mathbf{T}}\tilde{\mathbf{K}})} = \sqrt{\sum_{i=1}^{6}\sum_{j=1}^{6}\left|\tilde{\mathbf{K}}_{\mathbf{ij}}\right|^2} \tag{4}$$

$$\hat{\mathbf{K}} = \tilde{\mathbf{K}} / \left|\left|\tilde{\mathbf{K}}\right|\right|_F \tag{5}$$

Next, the normalized stiffness matrices are averaged over each group, by taking the mean value of each term, $\hat{\mathbf{K}}_\mathbf{G}$:

$$\hat{\mathbf{K}}_\mathbf{G} = \text{mean}(\hat{\mathbf{K}}_\mathbf{1}, \hat{\mathbf{K}}_\mathbf{2}, \ldots, \hat{\mathbf{K}}_\mathbf{N}) \tag{6}$$

where the subscript indicates the subject number.

Finally, we retrieve the scale and units for the group stiffness matrix. We retrieve the scale (de-normalize) by multiplying $\hat{\mathbf{K}}_\mathbf{G}$ by the mean of the Frobenius norms for the subjects in the group, $||\tilde{\mathbf{K}}_\mathbf{G}||$. Then the de-normalized stiffness matrix is de-dimension matched by pre-multiplying by $\mathbf{D_F^{-1}}$ and post multiplying by $\mathbf{D_X}$ to obtain the group average stiffness matrix, $\mathbf{K_G}$:

$$\left|\left|\tilde{\mathbf{K}}_\mathbf{G}\right|\right|_F = \text{mean}(\left|\left|\tilde{\mathbf{K}}_\mathbf{1}\right|\right|_F, \left|\left|\tilde{\mathbf{K}}_\mathbf{2}\right|\right|_F, \ldots, \left|\left|\tilde{\mathbf{K}}_\mathbf{N}\right|\right|_F) \tag{7}$$

$$\mathbf{K_G} = \mathbf{D_F^{-1}}(\left|\left|\tilde{\mathbf{K}}_\mathbf{G}\right|\right|_F \cdot \hat{\mathbf{K}}_\mathbf{G})\mathbf{D_X} \tag{8}$$

REFERENCES

[1] S. L. Weinstein, L. A. Dolan, J. G. Wright, and M. B. Dobbs, "Effects of bracing in adolescents with idiopathic scoliosis," *New England Journal of Medicine*, vol. 369, pp. 1512–1521, 2013.

[2] J. M. Carlson, "Clinical biomechanics of orthotic treatment of idiopathic scoliosis:," *Journal of Prosthetics and Orthotics*, vol. 15, pp. S17–S30, 2010.

[3] A. Jalalian, I. Gibson, and E. H. Tay, "Computational biomechanical modeling of scoliotic spine: Challenges and opportunities," *Spine Deformity*, vol. 1, pp. 401–411, 2013.

[4] A. Jalalian, F. E. H. Tay, S. Arastehfar, and G. Liu, "A new method to approximate load-displacement relationships of spinal motion segments for patient-specific multi-body models of scoliotic spine," *Medical & Biological Engineering & Computing*, vol. 55, pp. 1039–1050, 2017.

[5] J. P. Little and C. Adam, "Patient-specific computational biomechanics for simulating adolescent scoliosis surgery: Predicted vs clinical correction for a preliminary series of six patients," *International Journal for Numerical Methods in Biomedical Engineering*, vol. 27, pp. 347–356, 2011.

[6] S. P. S. B. I. T. N. Cobetto, C. E. Aubin and H. Labelle, "3D correction of AIS in braces designed using CAD/CAM and FEM: a randomized controlled trial," *Scoliosis Spinal Discord*, vol. 12, no. 24, 2017.

[7] C. Coillard, V. Vachon, A. B. Circo, M. Beauséjour, and C. H. Rivard, "Effectiveness of the SpineCor brace based on the new standardized criteria proposed by the scoliosis research society for adolescent idiopathic scoliosis," *Journal of Pediatric Orthopaedics*, vol. 27, pp. 375–379, 2007.

[8] T. B. Grivas, A. Bountis, I. Vrasami, and N. V. Bardakos, "Brace technology thematic series: the dynamic derotation brace," *Scoliosis*, vol. 5, p. 20, 2010.

[9] N. Nakamura, M. Uesugi, Y. Inaba, J. Machida, S. Okuzumi, and T. Saito, "Use of dynamic spinal brace in the management of neuromuscular scoliosis: a preliminary report," *Journal of Pediatric Orthopaedics*, vol. 23, pp. 291–298, 2003.

[10] J. P. A. Nijssen, G. Radaelli, J. L. Herder, C. J. Kim, and J. B. Ring, "Design and analysis of a shell mechanism based two-fold force controlled scoliosis brace," in *ASME 2017 International Design Engineering Technical Conferences and Computers and Information in Engineering Conference*, Cleveland, OH, 2017.

[11] S. D. Voinier, "Passive stiffness characteristics of the scoliotic lumbar torso in trunk flexion, extension, lateral bending, and axial rotation," Master's thesis, Virginia Polytechnic Institute, 2015.

[12] J. Park, P. R. Stegall, D. P. Roye, and S. K. Agrawal, "Robotic spine exoskeleton (RoSE): Characterizing the 3-d stiffness of the human torso in the treatment of spine deformity," *IEEE Transactions on Neural Systems and Rehabilitation Engineering*, vol. 26, pp. 1026–1035, 2018.

[13] N. Karavidas, "Bracing in the treatment of adolescent idiopathic scoliosis: Evidence to date," *Adolesc Health Med Ther*, vol. 10, pp. 153–172.

[14] J. Park, P. Stegall, and S. K. Agrawal, "Dynamic brace for correction of abnormal postures of the human spine," in *2015 IEEE International Conference on Robotics and Automation (ICRA)*, Seattle, WA, 2015, pp. 5922–5927.

[15] M. M. Panjabi, R. A. Brand, and A. A. White, "Three-dimensional flexibility and stiffness properties of the human thoracic spine," *Journal of Biomechanics*, vol. 9, pp. 185–192, 1976.

[16] M. H. Berkson, A. Nachemson, and A. B. Schultz, "Mechanical properties of human lumbar spine motion segments—-part II: Responses in compression and shear; influence of gross morphology," *Journal of Biomechanical Engineering*, vol. 101, pp. 53–57, 1979.

[17] A. B. Schultz, D. N. Warwick, M. H. Berkson, and A. L. Nachemson, "Mechanical properties of human lumbar spine motion segments—-part I: Responses in flexion, extension, lateral bending, and torsion," *Journal of Biomechanical Engineering*, vol. 101, pp. 46–52, 1979.

[18] M. G. Gardner-Morse and I. A. F. Stokes, "Structural behavior of human lumbar spinal motion segments," *Journal of Biomechanics*, vol. 37, pp. 205–212, 2004.

[19] B. D. Stemper, D. Board, N. Yoganandan, and C. E. Wolfla, "Biomechanical properties of human thoracic spine disc segments," *Journal of Craniovertebral Junction and Spine*, vol. 1, p. 18, 2010.

[20] O. M. O'Reilly, M. F. Metzger, J. M. Buckley, D. A. Moody, and J. C. Lotz, "On the stiffness matrix of the intervertebral joint: Application to total disk replacement," *Journal of Biomechanical Engineering*, vol. 131, pp. 081 007–1 – 081 007–9, 2009.